Appl Magn Reson (2010) 39:347–356
DOI 10.1007/s00723-010-0163-7

Applied
Magnetic Resonance

EPR/FMR Investigation of Mn-Doped SiCN Ceramics

S. I. Andronenko · Alfin Leo · I. Stiharu · Sushil K. Misra

Received: 15 February 2010 / Revised: 17 May 2010 / Published online: 26 September 2010

Abstract SiCN magnetic ceramics doped with Mn^{2+} ions were synthesized at the pyrolysis temperature of 1,100° C, using CERASET^{TM} as liquid polymer precursor and polymer manganese(II) acetylacetonate as dopant, and investigated by electron paramagnetic resonance (EPR)/ferromagnetic resonance (FMR) technique. The predominant source of ferromagnetism in SiCN samples doped with Mn ions, as synthesized here, is the ensemble of ferromagnetic nanoparticles of $Mn_5Si_3C_x$ incorporated into the amorphous SiC/Mn structure. The fluctuation of magnetization due to ferromagnetic $Mn_5Si_3C_x$ particles significantly broadens the EPR lines at the phase-transition temperature (363 K). This is the first fabrication of a SiCN/Mn ceramic, which exhibits room-temperature ferromagnetism.

1 Introduction

In the last few years, a new ceramic material, polymer-derived SiCN (silicon carbon nitride), has been exploited for microelectromechanical system (MEMS)

S. I. Andronenko A. Leo · I. Stiharu
Department of Mechanical and Industrial Engineering,
Concordia Centre for Advanced Vehicle Engineering, Concordia University,
1455 de Maisonneuve Boulevard West,
Montreal, QC H3G 1M8, Canada

Present Address:
S. I. Andronenko
Physics Department, Kazan Federal University, Kremlevskaya 18,
Kazan 420008, Russian Federation

S. K. Misra (✉)
Physics Department, Concordia University, 1455 de Maisonneuve Boulevard West,
Montreal, QC H3G 1M8, Canada
e-mail: skmisra@alcor.concordia.ca

applications. Simple and effective manufacturing technologies for this material have been developed using liquid–polymer precursor technique. SiCN ceramics, derived from liquid polyureasilazane precursor, have many outstanding physical properties, such as enhanced hardness, fracture strength, creep resistance and high functional temperature [1–3]. As well, these ceramics can be molded easily into very tiny and complicated shapes. These ceramics, fabricated above 1,000°C, have excellent thermal/mechanical properties for high-temperature/high-pressure applications. Mn-doped SiCN ceramics, referred to hereafter as SiCN/Mn, can be easily produced by addition of various manganese-containing compounds to the polymer precursor.

Superparamagnetic and ferromagnetic properties of SiCN/Mn ceramics can be exploited to fabricate spintronic devices [4], capable of withstanding extremely high temperatures. They become superparamagnetic in the nanostate characterized by very small crystallites (1–10 nm); as well, they become "soft" magnets due to their nanostructured nature, possessing very low coercivity with almost no magnetic hysteresis. They can be used very effectively as magnetic sensors being superparamagnetic. This is because very large changes in the magnetic flux density within them are produced by the application of a rather small magnetic field. Nanoparticles exhibit ferromagnetic behavior when their size is sufficiently large, wherein the internal crystalline part undergoes ferromagnetic ordering of paramagnetic ions, exhibiting ferromagnetic resonance (FMR) lines.

SiCN ceramics, potentially useful for MEMS applications, have been extensively investigated in the past few years [1–3, 5–22]. They consist of nanoparticles with the average size of 1.3 nm [5, 6, 9] when formed at pyrolysis temperatures of as low as 1,300°C as revealed by small-angle X-ray scattering (SAXS) [6]. On the other hand, at lower temperatures of synthesis, e.g., for the sample pyrolyzed at 1,000°C, the presence of carbon nanoparticles has been confirmed by the relative intensity of D and G bands in Raman spectra [9], with graphite nanoparticles of about 1 nm size being formed. Nanoparticles of such size can only be detected by SAXS method because their X-ray diffraction patterns are similar to those in the amorphous state, which show no peaks because their size is too small to exhibit Bragg's diffraction. The size of grains of thin films of SiCN ceramics, pyrolized at different temperatures from 900 to 1,600° C, is found to be anywhere from 5 to 50 nm depending upon the synthesis conditions [14].

The free-carbon phase in SiCN ceramics forms the so-called "cage" structure [15], proposed initially in the context of SiCO ceramics. Magnetic impurities, such as Mn composites, become incorporated in the SiCN nanoparticles. The Mn^{2+} magnetic moments couple with each other to produce superparamagnetism, or ferromagnetism, depending on their size.

Electron paramagnetic resonance (EPR) technique has been successfully used to investigate pure SiCN ceramic samples [7–13]. In particular, a detailed investigation of dangling bonds in these ceramics was carried out by EPR at several frequencies from 9.5 GHz to as high as 170 GHz at various temperatures from 4 to 300 K [7]. There was observed an intense EPR line due to carbon-related sp^2-dangling bonds [7–9], located on the surface of free-carbon phases with $g = 2.0027$. These dangling bonds were formed during ceramization, after which C–H bonds were broken, allowing for the formation of free-carbon phase. Recent confirmation of such origin

of this EPR signal was obtained by Tomasella et al. [11, 12]. Kobayashi et al. [13] reported EPR signal for ultraviolet-irradiated SiCN films. As for doped samples, so far, mainly SiCN ceramics doped with iron have been investigated [16–22]. Andronenko et al. [22] recently investigated the samples of SiCN ceramics doped with Fe by FMR/EPR, infrared and Raman spectroscopy, X-ray diffractometry and by measurements of magnetic properties. FMR/EPR spectroscopy was used for distinguishing different sources of magnetism in this material, finding at least three of them: (1) ferromagnetic $Fe_5Si_3C_x$ nanoparticles, (2) ferromagnetic clusters distributed in the free-carbon phase and, possibly, (3) Fe ions incorporated in SiCN nanoparticles, which can be formed at higher pyrolysis temperature, when crystallization of SiCN starts. Only one attempt has so far been made to synthesize SiCN/Mn composite by adding Mn metal powder to liquid CERASET^{TM} [21].

The purpose of this paper is to report the synthesis of SiCN/Mn ceramics, derived from liquid polyureasilazane precursor, using a manganese-containing polymer, and to provide a detailed X-band (9.5 GHz) EPR/FMR study of these samples in order to understand the various sources of their magnetism at variable temperatures. Manganese-containing polymers are believed to be the best sources for the synthesis of SiCN/Mn ceramics characterized by strong chemical bonding of manganese ions with the host ions of SiCN. In the present investigation, FMR signals were observed due to $Mn_5Si_3C_x$ nanoparticles and other magnetic impurities present in the SiCN/Mn composites, in addition to the EPR signals due to carbon-related dangling bonds and Mn clusters.

2 Synthesis of Mn-Doped SiCN Ceramics

The samples were prepared following the well-known process of fabrication of SiCN ceramics [1–3] using liquid precursor CERASET^{TM} polyureasilazane, to which 1 wt% of manganese(II) acetylacetonate $Mn(C_5H_7O_2)_2$ was added. It was mixed with 0.5 wt% of dicumyl peroxide to decrease thermosetting temperature to 160°C from the usual 220°C for pure CERASET^{TM}. This solution was then stirred for 2 h, and filtered to remove undissolved particles of powder to obtain a transparent dark-red liquid. The solution was poured inside a mold and thermoset at 160°C for 60 min under flowing nitrogen gas. Thereafter, the samples were removed from the mold and cross-linked at 400°C for 90 min to produce transparent dark-red solid polymer. This bonded the polymer chains of polyureasilazane into the polymer network, wherein the hydrogen ions were detached from the nitrogen ions, which became incorporated into the polymer chains bonding them together. The cross-linked polymer was then pyrolyzed at 1,100°C in the presence of nitrogen gas for 4 h with the heating rate of 4°C/min to yield solid ceramic samples. The pyrolysis eliminated excess carbon forming CH_4 molecules, and precipitated free carbon, leading to incorporation of some carbon ions into the mixed tetrahedral Si–C–N structure. Barnstead Thermolyne tube furnace F21135, with the maximum processing temperature of 1,200°C, was used for thermal treatments at 1,100°C. The composition of polymer-derived ceramics, as determined by elementary chemical analysis, was found to be $SiC_{0.68}N_{0.41}$ at pyrolysis temperatures of 1,100°C,

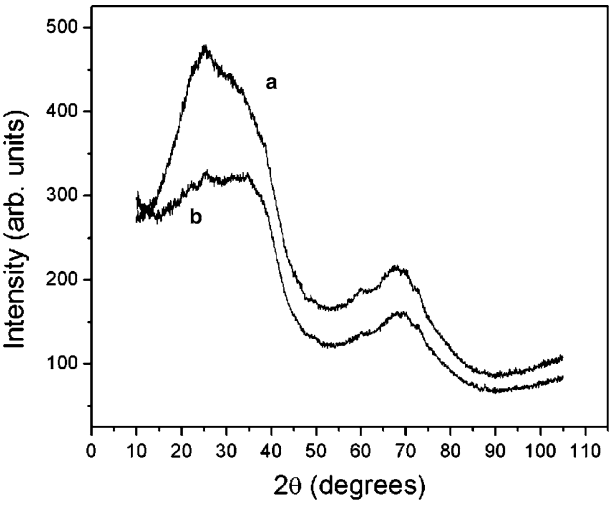

Fig. 1 X-ray diffraction patterns for SiCN/Mn samples: *a* samples doped with ~0.2% Mn, *b* samples doped with very small amount of Mn (<0.05%)

accompanied by 30 wt% of carbon in the free-carbon phase. Increasing the pyrolysis temperature led to increased removal of H atoms and formation of dangling bonds on the periphery of the free-carbon phase, as suggested by Trassl et al. [8, 9]. In addition, carbon-bonded dangling bonds were formed in the body of the SiCN ceramic network as defects. Finally, no oxygen was found to remain in the samples. The X-ray diffraction (XRD) pattern for the SiCN samples synthesized at 1,100°C is shown in Fig. 1. The samples are fully amorphous, since only very few peaks with very low intensity, mainly characterizing Si_3N_4 structure, have been observed. Two very broad peaks near 35° and 70° were ascribed to SiC nucleus, as suggested by Liew et al. [3]. No XRD peaks due to any Mn ions or Mn compounds were found here, indicating a rather negligible amount of Mn being present. It should be noted here that, as mentioned above, nanoparticles with very small size do not exhibit any XRD peaks. The concentration of Mn was found to vary from one sample to another, in the range 0.05–0.2% or less, according to neutron-activated analysis. Only the sample with the highest concentration of Mn (0.2%) was used here for FMR/EPR investigations.

Functional magnetic materials require a much higher Mn concentration than that present in the samples synthesized here in order to produce sufficient magnetization. Nevertheless, investigation of the SiCN/Mn ceramics, as produced here, is still important for understanding different sources of magnetism in these ceramics. Spintronic applications require simultaneous participation of spin and charge in spin dynamics and charge transfer in magnetic semiconductors. Therefore, further efforts are required to fabricate true diluted magnetic semiconductor materials, as well as functional magnetic and spintronic materials based on SiCN ceramics doped with transition metal ions.

3 EPR/FMR Investigations

A Bruker ER-200D SRC EPR X-band spectrometer equipped with Oxford helium-flow cryostat was used to investigate the SiCN/Mn ceramic samples in the temperature interval of 77–350 K. The EPR/FMR signals recorded at different temperatures are shown in Fig. 2. Variations of the resonance line positions, the intensity of the absorption signal (double-integrated intensity of the first-derivative EPR/FMR signal), and the line width (peak-to-peak line width of the first-derivative EPR/FMR signal) are shown in the temperature range 77–350 K in Figs. 3, 4 and 5, respectively.

3.1 FMR Lines

Inspection of Fig. 2 reveals the presence of a distinct FMR line (*A*) situated at ca. 650 G with a peak-to-peak width of ca. 800 G at room temperature, whose intensity increases with decreasing temperature. As well, it shows a structure on the lower magnetic field side with decreasing temperature. This line is due to the ferromagnetic particles of $Mn_5Si_3C_x$ present in the sample. In addition, adjacent to line A and situated to the right of it, there appears a powder-type FMR line, spread over a large magnetic field range ($\sim$1,000 to $\sim$2,700 G) due to randomly oriented ferromagnetic aggregates of varying shapes, sizes, and chemical compositions.

3.2 Critical Temperature as Determined from the FMR Line A

As the temperature was increased from 290 K, the area under the absorption line A, as obtained by double-integration of the first-derivative absorption curve, decreased

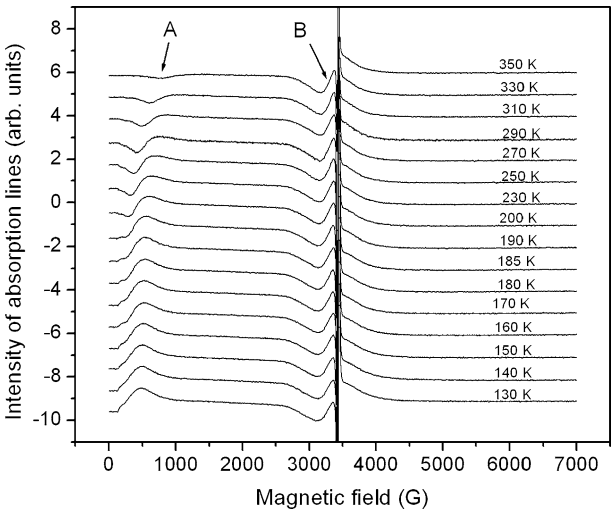

Fig. 2 Variation of the first-derivative signals with temperature. Here *A* and *B* are the FMR and the EPR signals, respectively, as described in Sect. 3

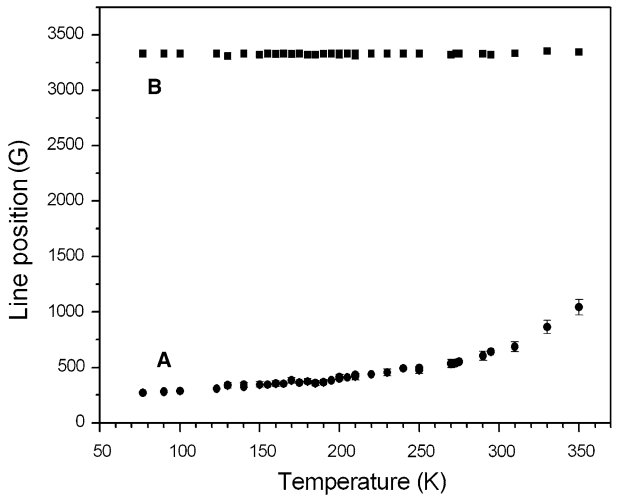

Fig. 3 Variation of the line positions with temperature for the FMR line *A* and the EPR line *B*

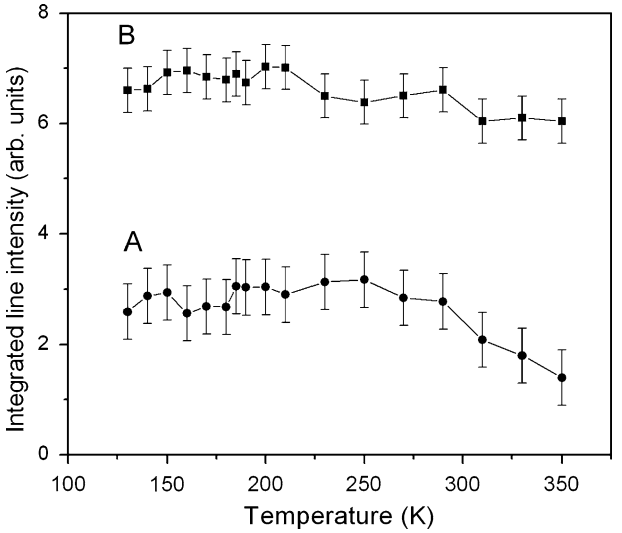

Fig. 4 Variation of the intensity (double-integrated first-derivative FMR line) on temperature for the lines *A* and *B*. The *continuous lines* connect experimental points

and approached zero at 350 K. This integrated intensity is proportional to the magnetization of the ferromagnetic $Mn_5Si_3C_x$ particles in the sample.

The FMR line width of line A was fitted to the following expression exhibiting the temperature (T) dependence [23]:

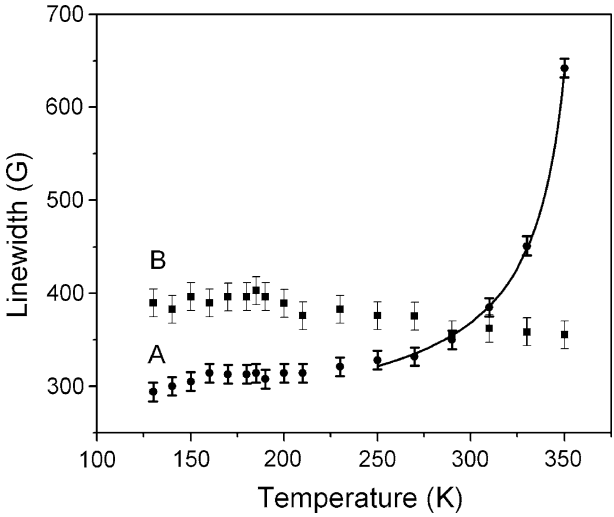

Fig. 5 Variation of the peak-to-peak first-derivative FMR line width with temperature for the lines *A* and *B*. The *continuous line* is that obtained by fitting with the parameters listed in Sect. 3

$$\Delta B = \Delta B_0 + A|T_c - T|^{-0.7}. \quad (1)$$

The fit yields the values $\Delta B_0 = (230 \pm 10)$ G, $A = (2.6 \pm 0.3) \times 10^3$ $K^{0.7}G$, and $T_c = (363 \pm 2)$ K. A considerable contribution to the FMR line width in ferromagnetic samples is due to the fluctuations of the magnetization, M, in the vicinity of the Curie temperature. Since the magnetization modifies the position of the resonance, its fluctuation produces broadening of the resonance line. The mean square of the fluctuation of the magnetization, following the theory of second-order phase transitions [24] and applying the scaling theory [25], can be expressed as:

$$\left\langle (\Delta M)^2 \right\rangle \propto |T_c - T|^{-1.4}, \quad (2)$$

where T_c is the critical temperature.

The EPR line width, ΔB, is proportional to the square-root of $\langle(\Delta M)^2\rangle$, the mean square of the fluctuation of the magnetization, M, in the vicinity of the phase transition as given by Eq. (1). This behavior is consistent with the temperature dependence of the magnetization of the ferromagnetic $Mn_5Si_3C_x$ ($x < 1$) particles characterized by the Curie temperature of 360 K, as deduced from the phase diagram of Mn–Si–C [26, 27].

3.3 EPR Lines

The EPR lines due to two different species were observed as described below.

1. *The EPR line due to dangling bonds* The sharp, narrow line at $g = 2.0026$ is due to dangling bonds. Its EPR line width, e.g., 1.4 G for the sample with

1 wt% of manganese(II) acetylacetonate in the Mn-doped sample, was found to be a bit larger than those in pure SiCN ceramic samples, e.g., 1.2 G in pure SiCN samples pyrolyzed at 1,100°C [7]. The extra contribution to the line width is due to the dipole–dipole interactions between carbon-related dangling bonds and the Mn^{2+} ions in the doped SiCN.

2. *The EPR line due to Mn clusters (B)* This rather broad line is situated at ca. 3,400 G ($g \sim 2.0$). The position of this line does not change in the temperature interval 360–400 K. It does not exhibit any significant temperature dependence of its line width or the double-integrated intensity over the temperature interval 77–350 K. The peak-to-peak EPR line width is ca. 350 G. This line is due to trace amounts of Mn clusters as revealed by its g value. (It is noted that the Mn^{2+} ion produces a strong signal, so that even trace amounts can exhibit a relatively intense line as observed presently.) The hyperfine splitting becomes unresolved due to dipolar interactions amongst Mn^{2+} ions, as well as due to inhomogeneous broadening.

4 Room-Temperature Magnetization

Further confirmation of the ferromagnetic behavior of SiCN/Mn sample was obtained here from the measurement of the magnetization of the sample with the content of Mn $\sim$0.2% at room temperature by a vibration sample magnetometer in the magnetic field range of 0–2.2 T. The results are shown in Fig. 6. The hysteresis loop indicates a "soft"-mode magnetization with the saturation magnetic field of $\geq$0.4 T. The associated coercive field is $\leq$10 mT for the SiCN/Mn samples. It is clearly seen in Fig. 6 that at room temperature SiCN/Mn is purely ferromagnetic.

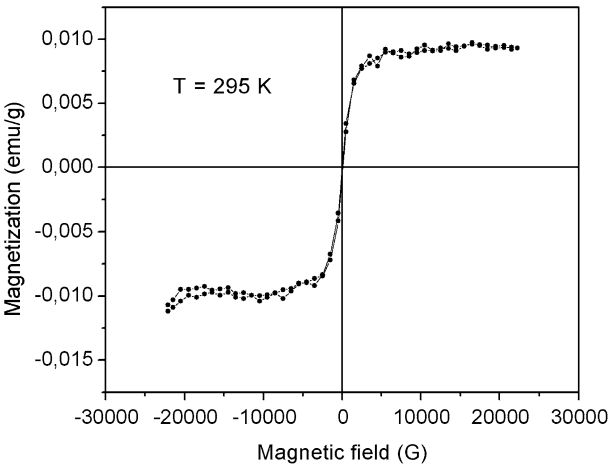

Fig. 6 Hysteresis curve showing the dependence of the magnetization of SiCN/Mn ceramics on the magnetic field at 295 K

Pure undoped SiCN samples are diamagnetic and the susceptibility was measured to be $\chi_{dia} = -0.38 \times 10^{-6}$ emu/g.

5 Discussion and Concluding Remarks

Although the SiCN/Mn sample investigated here contains a rather small concentration of Mn ($\sim$0.2%), the FMR and magnetization data show that the ferromagnetic behavior is due only to ferromagnetic nanoparticles. Coupled Mn ions are produced by the specific method used here for the synthesis of SiCN/Mn ceramics. During the first step of synthesis, Mn(II) acetylacetonate powder was added to liquid CERASET^{TM} polymer. Although this powder was dissolved and filtered, some small particles still remained undissolved, serving as centers for nucleation of magnetic clusters, so that ferromagnetic particles of $Mn_5Si_3C_x$, or other composites, are formed during pyrolysis. On the other hand, superparamagnetic clusters could be formed when these particles are less than 5 nm in size. However, in that case, the magnetization does not exhibit the Curie-law behavior, as deduced from the temperature dependence of the double-integrated intensity of the FMR line, being proportional to the magnetization. This indicates that there are no paramagnetic or superparamagnetic particles present in the sample. This is due to poor solubility of Mn(II) acetylacetonate powder in CERASET^{TM}, which leads to the formation of rather large particles, exhibiting ferromagnetic behavior due to their size.

The two different composites of Mn ions are: (1) localized ferromagnetic nanoparticles related mainly to SiC amorphous matrix, which is formed at the initial step of SiCN synthesis, with the composition (Mn–Si–C); and (2) nanoparticles related to the formation of SiCN network (Mn–Si–N–C). The first kind of nanoparticles relate to the formation of $Mn_5Si_3C_x$ nanoparticles, as deduced here from the temperature dependence of the FMR line A. These particles exhibit a transition from ferromagnetic to paramagnetic phase at 363 K. This can be easily understood, since at 1,100°C the nucleus of SiC begins to appear, as revealed by XRD patterns. The second kind of nanoparticles relate mainly to clusters of manganese ions, incorporated into the Si–C–N tetrahedron [10], responsible for the EPR line B.

The present FMR investigations clearly prove the existence of ferromagnetic nanoparticles, distributed over the diamagnetic SiCN ceramic structure. From strong changes in the FMR line width and line position with temperature, one can identify these particles to be $Mn_5Si_3C_x$.

The room-temperature ferromagnetism in SiCN ceramics doped with Mn was accomplished for the first time in this work. Additional investigations of SiCN/Mn ceramics, annealed at different temperatures, are required to plot the magnetic phase diagram of SiCN ceramics doped with Mn ions.

Acknowledgments S.A. and I.S. are grateful for support from Consortium de Recherché et d' Innovation en Aerospatiale au Quebec (CRIAQ) and Pratt and Whitney, Canada. S.K.M. is grateful for

partial financial support from the Natural Sciences and Engineering Research Council (NSERC) of Canada. Thanks are due Prof. D. Menard for magnetic properties measurements.

References

1. L.-A. Liew, W. Zhang, V.M. Bright, L. An, M.L. Dunn, R. Raj, Sens. Actuators A **89**(1–2), 64–70 (2001)
2. L.-A. Liew, Y. Liu, R. Luo, T. Cross, L. An, V.M. Bright, M.L. Dunn, J.W. Daily, R. Raj, Sens. Actuators A **95**(2–3), 120–134 (2002)
3. L.-A. Liew, R.A. Saravanan, V.M. Bright, M.L. Dunn, J.W. Daily, R. Raj, Sens. Actuators A **103**(1–3), 171–181 (2003)
4. S.A. Wolf, D.D. Awschalom, R.A. Buhrman, J.M. Daughton, S. von Molnár, M.L. Roukes, A.Y. Chtchelkanova, D.M. Treger, Science **294**(5546), 1488–1495 (2001)
5. J. Bill, T.W. Kamphowe, A. Muller, T. Wichmann, A. Zern, A. Jalowieki, J. Mayer, M. Weinmann, J. Schuhmacher, K. Muller, J.Q. Peng, H.J. Seifert, F. Aldinger, App. Organomet. Chem. **15**(10), 777–793 (2001)
6. A. Saha, R. Raj, D.L. Williamson, H.-J. Kleebe, J. Am. Ceram. Soc. **88**(1), 232–234 (2005)
7. S.I. Andronenko, I. Stiharu, S.K. Misra, J. Appl. Phys. **99**, 113907 (1–5) (2006)
8. S. Trassl, G. Motz, E. Rossler, G. Ziegler, J. Am. Ceram. Soc. **85**(1), 239–244 (2002)
9. S. Trassl, H.-J. Kleebe, H. Stormer, G. Motz, E. Rossler, G. Ziegler, J. Am. Ceram. Soc. **85**(5), 1268–1274 (2002)
10. Y.-L. Li, E. Kroke, R. Riedel, C. Fasel, C. Gervais, F. Babonneau, Appl. Organometal. Chem. **15**(11), 820–832 (2001)
11. E. Tomasella, L. Spinelle, A. Bousquet, F. Rebib, M. Dubois, C. Eypert, J.P. Gaston, J. Cellier, Plasma Process. Polym. **6**(21), S11–S16 (2009)
12. E. Tomasella, F. Rebib, M. Dubois, J. Cellier, M. Jacquet, J. Phys. Conf. Ser. **100**, 082045 (2008)
13. K. Kobayashi, H. Yokoyama, M. Endoh, Appl. Surf. Sci. **254**(19), 6222–6225 (2008)
14. A. Leo, S. Andronenko, I. Stiharu, R.B. Bhat, Sensors **10**(2), 1338–1354 (2010)
15. A. Saha, R. Raj, J. Am. Ceram. Soc. **90**(2), 578–583 (2007)
16. A. Saha, S.R. Shah, R. Raj, S.E. Russek, J. Mater. Res. **18**(11), 2549–2551 (2003)
17. J. Li, Z. Zhang, Z. Zheng, L. Guo, G. Xu, Z. Xie, J. Appl. Polym. Sci. **105**(4), 1786–1792 (2007)
18. M.J. MacLachlan, M. Ginzburg, N. Coombs, T.W. Coyle, N.P. Raju, J.E. Greedan, G.A. Ozin, I. Manners, Science **287**(5457), 1460–1463 (2000)
19. A. Dumitru, I. Stamatin, A. Morozan, C. Mirea, V. Ciupina, Mater. Sci. Eng. C **27**(5–8), 1331–1337 (2007)
20. Y. Li, Z. Zheng, C. Reng, Z. Zhang, W. Gao, Z. Xie, Appl. Organometal. Chem. **17**(2), 120–126 (2003)
21. X.H. Yan, X.N. Cheng, G.C. Han, R. Hauser, R. Riedel, Key Eng. Mat. **353–358**, 1485–1488 (2007)
22. S.I. Andronenko, I. Stiharu, D. Menard, C. Lacroix, S.K. Misra, Appl. Magn. Res., **38**(4), 385–402 (2010)
23. T.S. Altshuler, M.S. Bresler, Yu. V. Goryunov, JETP Lett. **81**(9), 475–478 (2005)
24. L.D. Landay, E.M. Lifshitz, *Course of Theoretical Physics, v.5.: Statistical Physics*, 3rd edn. (Pergamon Press, Oxford, 1980)
25. A.Z. Patashinskii, V.L. Pokrovskii, *Fluctuation Theory of Phase Transitions* (Pergamon Press, Oxford, 1979)
26. C. Sürgers, K. Potzger, G.S. Fischer, J. Chem. Sci. **121**(2), 173–176 (2009)
27. B. Gopalakrishnan, C. Sürgers, R. Montbrun, A. Singh, M. Uhlarz, H. Löhneysen, Phys. Rev. B **77**, 104414 (2008)